

SYNTHESIS AND CHARACTERIZATION OF BIO-COMPATIBLE MAGHEMITE NANOPARTICLES

D. PREDOI^{a*}, E. ANDRONESCU^b, M. RADU^c, M. C. MUNTEANU^c, A. DINISCHIOTU^c

^aNational Institute of Materials Physics, Atomistilor 105 Bis, P.O. Box. MG 07, 077125, Magurele, Romania

^bUniversity POLITEHNICA of Bucharest, Faculty of Applied Chemistry and Materials Science, Department of Science and Engineering of Oxide Materials and Nanomaterials, 1-7 Polizu Street, P.O. Box 12-134, 011061 Bucharest, Romania

^cDepartment of Biochemistry and Molecular Biology, University of Bucharest, 91-95 Splaiul Independenței, 050095, Bucharest 5, Romania

The bio-compatible magnetic nanoparticles of maghemite were prepared by a chemical co-precipitation method and dextran was selected as the surfactant to suspend them. By transmission electron microscopy (TEM), the iron oxide nanoparticles appeared nearly spherical with an average diameter of about 8.0 ± 1 nm. SAED pattern of iron oxide nanoparticles is indexed by a cubic γ -Fe₂O₃, the diffraction rings are attributed to the (220), (311), (400), (422), (511) and (440) planes, respectively. Regular fringes are clearly observed in the nanoparticle with a spacing of 0.24 nm, which is the (311) interplanar distance of the cubic maghemite. This is in perfect agreement with the X-Ray Diffraction (XRD) results, indicating that the nanoparticles are well crystallized in spite of their ultrafine sized. The attachment of the dextran on the particle surface was confirmed by Fourier Transform Infrared (FTIR) Spectroscopy. The biocompatibility of maghemite nanoparticles covered by dextran with HepG2 cells was checked by MTT test. Cell viability was > 98% when the iron concentration was 12.0 μ g iron/ml and 24.0 μ g iron/ml respectively. In conclusion, these nanoparticles presented a good biocompatibility with HepG2 cells, which was proportionally with the dilution level.

(Received August 14, 2010; accepted September 14, 2010)

Keywords: Maghemite, Co-precipitation, Nanoparticles, Dextran

1. Introduction

Functionalized magnetic nanoparticles are used in several biomedical applications, such as drug delivery, magnetic cell separation and magnetic resonance imaging (MRI), contrast agents for diagnostics. Although there are several kinds of interesting magnetic nanoparticles, iron-oxide particle magnetite (Fe₂O₃) and its oxidized form maghemite (γ -Fe₂O₃) have attracted more attention because they are non-toxic and less susceptible to change due to oxidation. These facts make this kind of nanoparticles one of the most studied materials for biomedical applications [1-2].

The study of nanoscale magnetic materials domains is of both fundamental and pressing technical interest as the grain size of advanced recording media is rapidly shrinking to dimensions where as an example the magnetic properties depend strongly on nanocrystal size [3] with their characteristic size in the range 1-100 nanometers.

The diagnostic and therapeutic applications of magnetic iron-oxide nanoparticles (MNP) are underlined above expanded enormously in the past decades. Magnetic resonance imaging

* dpredoi68@gmail.com

(MRI) provides excellent differential soft-tissue contrast in order to discriminate between healthy tissue and abnormalities such as tumors [4-5]. In oncology, magnetic nanoparticle (MNP) are being used to aid in disease staging, treatment planning, and assessing tumor response to therapy [5]. In order to address the problems of short half-life and rapid clearance in the reticuloendothelial system (RES) MNPs are modified with various surface coatings, such as dextran, starch, citrate or synthetic polymers [5].

In order to ensure stability and reproducible performance of biocompatible colloids based on iron oxide nanoparticles it is important to monitor and control their composition and uniformity [6]. Stability, biocompatibility and relaxometric properties of these iron oxide colloids are affected by their particle size distribution as well as by the surface coating of the particles in the solution [6-7]. The most common coatings for biocompatible iron oxide based colloids are derivatives of dextran, a polyethylene glycol [6].

This work expresses the effort to understand the nature of the interaction of dextran with iron oxide surface due to its importance in affecting the residence time of the nanoparticles in the blood before its clearance, and, therefore, its actuation time.

This work describes the synthesis and physical characterization using X-ray diffraction (XRD), transmission electron microscopy (TEM) of the spherical magnetic spinel iron oxide nanoparticles. Dextran attachments were put into evidence by FTIR and thermal analysis (TG/DTA). The biocompatibility of iron oxide coated with dextran, was assessed by Hep G2 cell viability and morphology. The cytotoxicity of maghemite nanoparticles covered by dextran on HepG2 cells was checked by MTT test.

2. Experimental

Synthesis of iron oxide ferrofluid. Maghemite nanoparticles were prepared by coprecipitation according to [8-11]. Ferrous chloride tetrahydrate ($\text{FeCl}_2 \cdot 4\text{H}_2\text{O}$) in 2M HCl and ferric chloride hexahydrate ($\text{FeCl}_3 \cdot 6\text{H}_2\text{O}$) were mixed at 100°C ($\text{Fe}^{2+}/\text{Fe}^{3+} = 1/2$). The mixture was dropped into 200 ml of NaOH ($2 \text{ mol} \cdot \text{L}^{-1}$) solution under vigorous stirring for about 30 min. The precipitate of magnetite (black precipitate immediately formed) was converted into $\gamma\text{-Fe}_2\text{O}_3$ particles by repeated treatment with HNO_3 ($2 \text{ mol} \cdot \text{L}^{-1}$) and FeNO_3 ($0.3 \text{ mol} \cdot \text{L}^{-1}$) solutions in according to [11-12]. The acidic precipitate was isolated by decantation on a magnet, separated by centrifugation (6000 rpm), washed in acetone and dispersed in deionized water at $\text{pH}=2.5$. In a final step, the obtained product was mixed at various ratios with the different polymer solutions to obtain either iron oxide coated with dextran. For biological investigations, the pH was adjusted to 7 using aqueous ammonia. The iron content of the suspensions was determined by redox-titration, essentially as described [13]. The samples were investigated for polymer/iron mass ratio $r = 20$.

Transmission Electron Microscopy (TEM). TEM studies were carried out using a JEOL 200 CX. The specimen for TEM imaging was prepared from the particles suspension in deionized water. A drop of well-dispersed supernatant was placed on a carbon – coated 200 mesh copper grid, followed by drying the sample at ambient conditions before it is attached to the sample holder on the microscope.

X-Ray Diffraction (XRD). The samples were characterized for phase content by X-ray diffraction (XRD) with a Bruker D8-Advance X-ray diffractometer in the scanning range $2\theta = 15 - 140$ using $\text{CuK}_{\alpha 1}$ incident radiation.

Thermogravimetric analysis. The thermal behaviour of the powders was studied by differential thermal analysis (DTA) and thermal gravimetric analysis (TGA) using a Shimadzu DTG-TA-50 and DTA 50 analyzer in the $25\text{-}800^\circ\text{C}$ temperature range, air environment, and Al_2O_3 reference. Temperature increasing rate is $5^\circ\text{C}/\text{min}$.

Fourier Transform Infrared (FTIR) Spectroscopy. The functional groups present in the prepared powder and in the powders calcined at different temperatures were identified by FTIR (Spectrum BX Spectrometer). For this 1% of the powder was mixed and ground with 99% KBr. Tablets of 10 mm diameter for FTIR measurements were prepared by pressing the powder mixture at a load of 5 tons for 2 min and the spectrum was taken in the range of 400 to 4000 cm^{-1} with resolution 4 and 128 times scanning.

Cell culture and treatment. Hep G2 cells were maintained in DMEM, containing 3,7 g/L sodium bicarbonate, 4,5g/L D-glucose, 4,7g/L 4-(2-hydroxyethyl)-1-piperazineethanesulfonic acid (HEPES), 4 mM L-glutamine, 0,1 mM sodium pyruvate, 100 U/ml penicillin, 100 U/ml streptomycin and 10% (v/v) foetal bovine serum. Cells were grown in 5% CO₂ at 37°C. The cells were grown as monolayers in 75 cm² cell culture flasks. They were seeded at a density of 2,5x10⁵ cells/ml and incubated with the maghemite nanoparticles at different iron concentration (0.0 µg iron/ml, 12.0 µg iron /ml, 24.0 µg iron /ml, 60.0 µg iron /ml and 240 µg iron /ml) for 24 hours.

Cell viability. The cell viability was determined by the MTT test [14]. The medium from each well was removed by aspiration, the cells were washed with 200 µl phosphate buffer solution (PBS)/well and then 50µl (1mg/ml) 3-(4,5-dimethylthiazol-2-yl)-2,5-diphenyltetrazolium bromide (MTT) solution was added on each well. After 2 hours of incubation the MTT solution from each well was removed by aspiration. A volume of 50 µl isopropanol was added and the plate was shaken to dissolve formazan crystals. The optical density at 595nm, for each well, was then determined using a Tecan multiplate reader (Tecan GENios, Grödic, Germany).

Morphology. The cells were plated at day one at a density of 5x10⁴cells/cm² on flasks. After 24 h, the cells were imaged by a bright field inverted microscope (Olympus IX7). Images were acquired by specific software Cell F using a CCD video camera COLORVIEW.

3. Results and discussion

The maghemite nanoparticles synthesised by coprecipitation method as shown in Figure 1 (A). It can be seen that the particles are well dispersed and aggregation is minimal. These monodisperse nanoparticles have an average grain size of 8.3±0.3 nm. Grain size distribution were determined by measuring the mean diameter, D, of ca. 500 particles on the micrographs (Figure 1 (E)). The high-resolution TEM image in Figure 1 (B) shows the internal crystallinity for an iron oxide nanocrystal. Regular fringes are clearly observed in the nanoparticle with a spacing of 0.24 nm, which is the (311) interplanar distance of the cubic maghemite. SAED pattern of iron oxide nanoparticles in Figure 1 (C) is indexed by a cubic γ -Fe₂O₃ (PCPDF#872334), the diffraction rings are attributed to the (220), (311), (400), (422), (511) and (440) planes, respectively. Figure 1 (D) shows typical TEM images from maghemite nanoparticles coated with dextran. TEM images indicate a very uniform size distribution of dextran coated maghemite nanoparticles. This is in perfect agreement with the XRD results to be presented below (Figure 2), indicating that the nanoparticles are well crystallized in spite of their ultrafine sized.

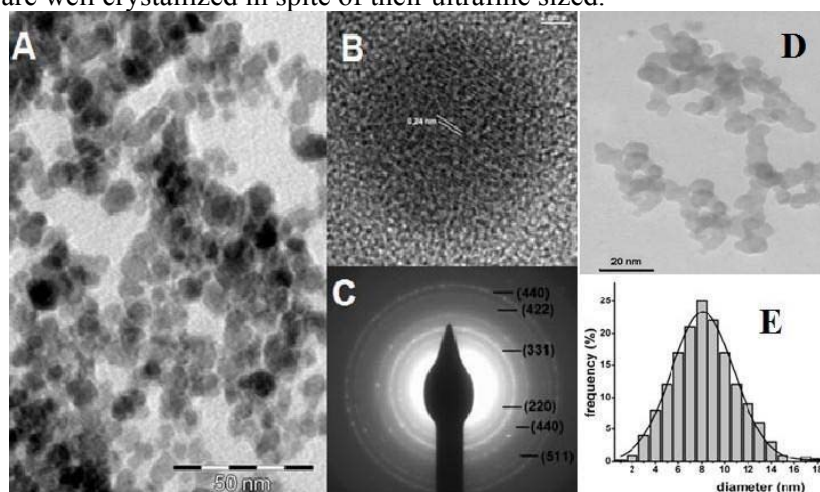


Fig. 1. Synthesized maghemite nanoparticles dispersed in aqueous solution. Large area TEM image (A), High Resolution TEM image (B) and SAED pattern (C), synthesized dextran coated maghemite nanoparticles dispersed in aqueous solution (D), size distribution of iron oxide nanoparticles (E).

The diffraction pattern (Figure 2) shows the peaks that corresponds to an fcc cubic maghemite structure (ICSD card no.01-083-0112). The lattice parameter is 0.836 nm. The line broadening is essentially due to the size effect. The average size (7.8 nm), deduced from the full

width at half maximum, are consistent with the mean sizes deduced from TEM observations. The average sizes $\langle D \rangle$ of the nanoparticles were computed using Scherrer's formula [15]:

$$D = K\lambda/B \cos\theta$$

where D is the averaged length of coherence domains (that is of perfectly ordered crystalline domains) taken in the direction normal to the lattice plane that corresponds to the diffraction line taken into account, B is the line broadening due to the small crystallite size, λ is the wavelength of X-rays (1.5416 Å), θ is the Bragg angle, and K a constant related to crystallite shape and to the definition of B (integral breadth or full width at half maximum).

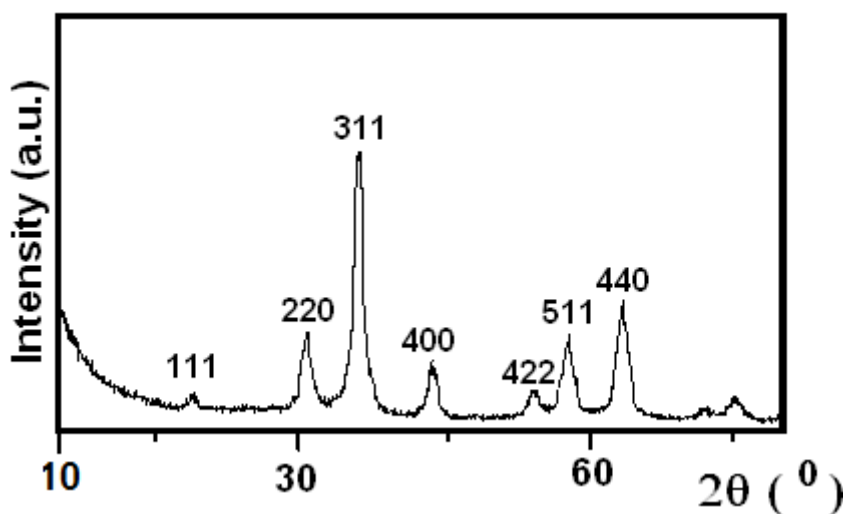


Fig. 2. X-Ray diffraction pattern of samples of maghemite nanoparticles.

Fig. 3 shows the weight loss curves obtained using a thermogravimetric analyzer. For the dextran coated iron oxide nanoparticles two weight loss stages were observed in thermograms. The first weight loss is due to the evaporation of water. The other stage beginning at about 300°C is due to the decomposition of dextran.

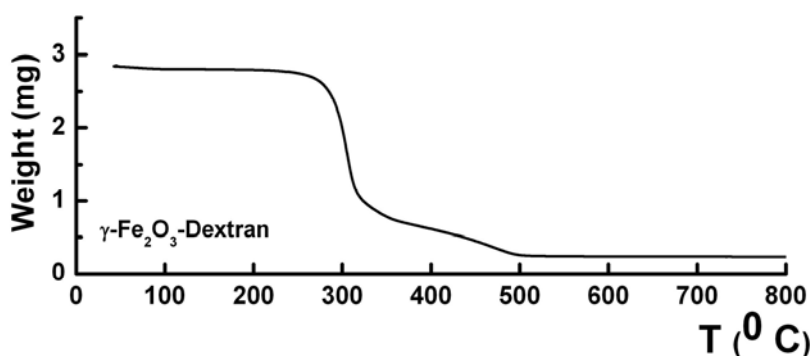


Fig. 3. Weight loss curves of dextran coated iron oxide nanoparticles at a temperature increasing rate of 5°C/min, in the range from 25°C to 800°C.

Fig. 4 illustrates the FT-IR spectra of different samples (iron oxide nanoparticles, dextran coated iron oxide and dextran). The spectrum of the iron oxide contains characteristic OH stretching (ν OH) and HOH bending (δ OH) vibrational bands at 3400 cm^{-1} and 1600 cm^{-1} due to the adsorbed water in the sample [16]. From the spectrum of iron oxide, we found that the bands observed at 620 cm^{-1} and 580 cm^{-1} corresponds to the stretching vibration MTh- O-MOh. The band

at about 400 cm^{-1} corresponds to the stretching vibration. MTh and MOh correspond to the metal occupying tetrahedral and octahedral positions respectively [17-19]. The stretching vibration $\nu(\text{Fe-O})$ correspond of tetrahedral iron atoms.

The spectral range $1000\text{-}1200\text{ cm}^{-1}$ were due to $\nu(\text{C-C})$ and $\nu(\text{C-O})$ stretching vibration with contributions from $\delta(\text{C-O-H})$ motion [20]. We suggested that the band centred at 1159 cm^{-1} could be assigned to $\delta(\text{C-O-H})$. The vibrational bands at 1013 and 1045 cm^{-1} in the spectrum of dextran have been assigned to the $\nu(\text{C-O})$ vibration with contributions from $\nu(\text{C-OH})$, $\nu(\text{C-C})$ and $\delta(\text{C-O-H})$ modes. It has been suggested that the absorption bands in spectral range between 1200 and 1500 cm^{-1} may be caused mainly by CH deformation vibrations and $\delta(\text{COH})$ bending vibrations. The spectrum shows one mode around 1273 cm^{-1} assigned to the $\nu(\text{C-O})$ stretching mode in the ring [21]. The normal mode at 1360 cm^{-1} is an almost pure $\delta(\text{C-O-H})$ vibration and the mode at 1429 and 1460 cm^{-1} a pure CH_2 group vibration. We assigned the bands present at 2935 and 3429 cm^{-1} $\nu(\text{C-H})$ and $\nu(\text{O-H})$ stretching vibration [22].

Comparing Figure 4, characteristic vibrations of CH, C-O-C, COH were found in dextran coated iron oxide nanoparticles.

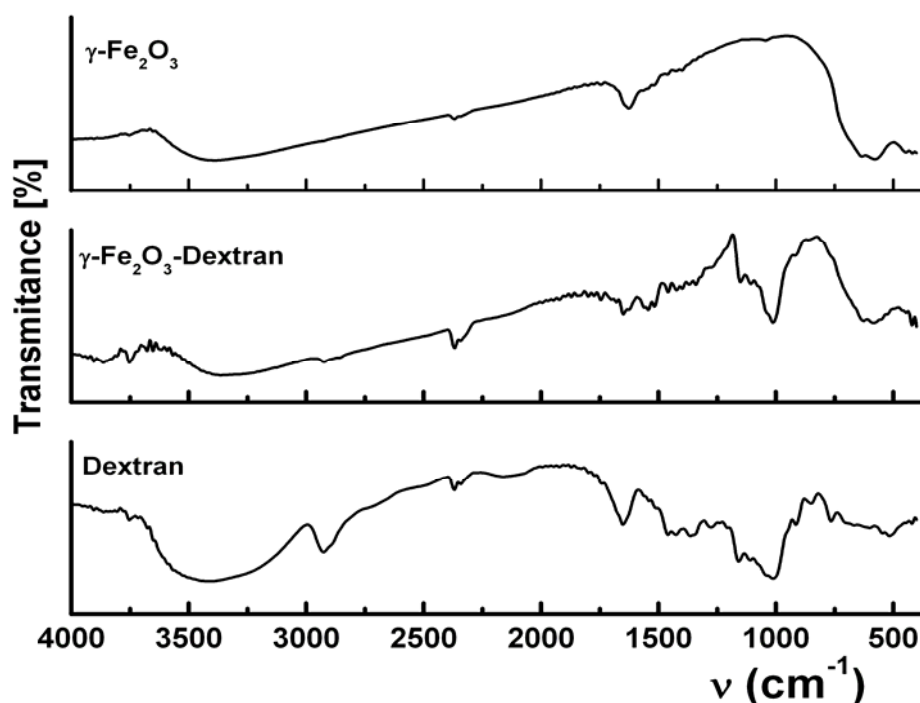


Fig. 4. FT-IR spectra of $\gamma\text{-Fe}_2\text{O}_3$, dextran coated $\gamma\text{-Fe}_2\text{O}_3$ and pure dextran.

In order to evaluate the compatibility degree of maghemite nanoparticles coated with dextran with HepG2 cells, the MTT test for 24 hours was performed for different iron concentration. We compared the cytotoxicity at long time (24h) exposure of HepG2 cells to iron oxide nanoparticles coated with dextran at varying iron concentration ($0.0\text{ }\mu\text{g iron/ml}$, $12.0\text{ }\mu\text{g iron/ml}$, $24.0\text{ }\mu\text{g iron/ml}$, $60.0\text{ }\mu\text{g iron/ml}$ and $240\text{ }\mu\text{g iron/ml}$) (Figure 5). The viability of cells in the presence of maghemite nanoparticles coated with dextran was lower compared to control samples with the same iron concentration ($60.0\text{ }\mu\text{g iron/ml}$ and $240\text{ }\mu\text{g iron/ml}$). Cell viability was $> 98\%$ when the iron concentration was $12.0\text{ }\mu\text{g iron/ml}$ and $24.0\text{ }\mu\text{g iron/ml}$ respectively.

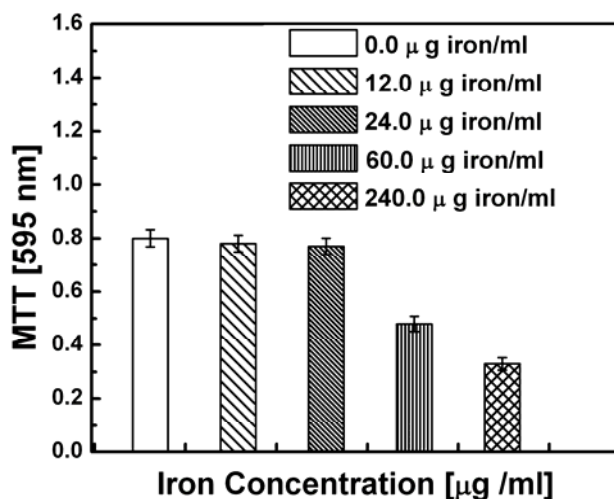


Fig. 5. Cytotoxicity of the various iron concentration for HepG2 cells. The cells were exposed for 24 h, then viability was determined using the MTT assay.

Firstly, we investigated the impact of the observed differences in iron oxide nanoparticles architecture on HepG2 cells morphology and viability. The cells have a typical polygonal morphology. After 24 h exposure to all types of iron oxide nanoparticles coated with dextran at varying iron concentration the polygonal morphology was preserve. Cell viability assay showed that HepG2 cells culture on iron oxide coated with dextran were viable for up to 60.0 µg iron /ml after 24h and could properly attach to all substrata without any sign of cell death (Figure 6 B-C). Morphological differences in cell aggregation on iron oxide nanoparticles coated with dextran were observed by progressive structural alterations and reductions of HepG2 cell population (Figure 6 D-E).

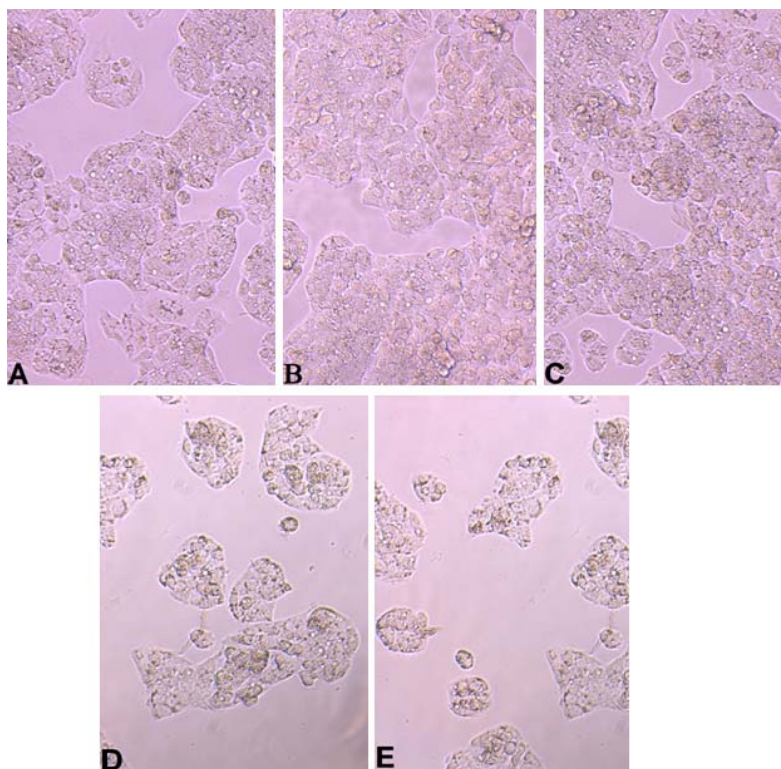


Fig. 6. Morphological comparison of HepG2 cells on iron oxide nanoparticles coated with dextran at varyng iron concentration: 0.0 µg iron/ml (A), 12.0 µg iron /ml (B), 24.0 µg iron /ml (C), 60.0 µg iron /ml (D) and 240 µg iron /ml (E).

The MTT-assay was used to measure iron oxide induced changes in viability of HepG2 cells. The HepG2 cell line is easy to handle and provides a reproducible human system. For predict metabolism in adult human liver cells further studies on the primary hepatocytes are in progress.

4. Conclusions

The iron oxide nanoparticles with a mean diameter of 8.3 nm and a narrow particle size distribution (~ 1-18 nm) have been synthesized by coprecipitation of $\text{FeCl}_2 \cdot 4\text{H}_2\text{O}$ and $\text{FeCl}_3 \cdot 6\text{H}_2\text{O}$ ($\text{Fe}^{2+}/\text{Fe}^{3+} = 1/2$) in NaOH ($2 \text{ mol} \cdot \text{L}^{-1}$) at 100°C . As the XRD and TEM investigations, the maghemite phase was obtained. FT-IR analysis of dextran coated iron oxide reveals that the dextran is present at the surface of the nanoparticles. The abundant surface hydroxyl group allow the nanoparticles to be coated with dextran.

MTT assay cell viability shows that the iron oxide nanoparticles coated with dextran have good biocompatibility when the iron concentration is lower to $60.0 \mu\text{g iron/ml}$ for a polymer/iron mass ratio $r = 20$. These studies enabled us to understand the interactions of these nanoparticles with cells in vitro conditions. With further surface modifications by conjugating some bioactive molecules, macromolecules, to those nanoparticles, the obtained maghemite nanoparticles will provide a profound base for future discussions on toxicity and potential applications of nanoparticles in the field of biomedicine.

Acknowledgements

This work was financially supported by Science and Technology Ministry of Romania (PNCDI II 71-097/2007, PN II IDEI/340/2007).

References

- [1] A.K. Gupta, M. Gupta, *Biomaterials*, **26**, 3995 (2005).
- [2] Chen Qin, Chen Li, Yizhe Hu, Jiarfeng Shen, Mingxin Ye, *Colloids and Surfaces A: Physicochem. Eng. Aspects*, **336**, 130 (2009).
- [3] G.Q. Zhang, H.P. Wu, M.Y. Ge, Q.K. Jiang, L.Y. Chen, J.M. Yao, *Materials Letters*, **61**, 2204 (2007).
- [4] Yuqing Ge, Yu Zhang, Jinjguang Xia, Ming Ma, Shiyang He, Fang Nie, Ning Gu, *Colloids and Surfaces B: Biointerfaces*, **73**, 294 (2009)
- [5] Tapan K. Jain, Susan P. Fay, Bernadette Erokwu, Sanja Dimitrijevic, Christopher A. Flask, Vinad Labhasetwar, *Biomaterials* **30**, 6748 (2009).
- [6] M. Carmen Bautista, Oscar Bomati-Miguel, Maria del Puerto. Morales, Carlos J. Serna, Sabrina Veintemillas-Verdaguer, *Journal of Magnetism and Magnetic Materials* **293**, 20 (2005).
- [7] U. Häfeli, W. Schiit, J.Teller, M. Zborowski *Scientific and Clinical Application of Magnetic Carriers* Plenum Press New York ,1997
- [8] R. Massart, *Brevet francais*, **79**, 18842(1979); U.S. Patent **4**(329), 241 (1982).
- [9] R. Massart, *IEEE Trans. Magn.* **17**, 1247 (1981).
- [10] A. Bee, R. Massart, *J. Magn. Mater.* **1**, 122 (1990).
- [11] D. Predoi, C. Valsangiacom, *J. Optoelectron. Adv. Mater.* **9**(6), 1797 (2007)
- [12] S. Mornet, F. Grasset, J. Portier, E. Duguet, *European Cells and Materials* **3**(2), 110 (2002).
- [13] D.A. Skoog, *Fundamentals of analytical chemistry*. Fort worth: Saunders College Publishing, 1999
- [14] J. Mosmann, *J. Immunol Methods* **65**, 55 (1983).
- [15] R. M. Cornell, U. Schertmann, *Iron Oxides in the Laboratory: Preparation and Characterisation*, VCH, Weinheim, 1991.
- [16] M. L. Hair, *J. Non-Cryst. Solids* **19**, 299 (1975).
- [17] E. Barrodo, F. Prieto, J. Medina, F. A. Lopez, *J. Alloys. Compd.* **335**, 203 (2002).

- [18] J. L. Martin de Vidales, A. Lopez-Delgado, E. Vila, F. A. Lopez, *J. Alloys. Compd.* **287**, 276 (1999).
- [19] D. Predoi, *Digest Journal of Nanomaterials and Biostructures* **2**(1), 169 (2007).
- [20] J. Hradil, A. Pisarov, M. Babič, D. Horák, *China Particuology* **5**, 162 (2007)
- [21] H. R. Wang, K. M. Chen, *Colloids and Surfaces A: Physicochem. Eng. Aspects* **281**, 190 (2006).
- [22] E. Castellanos Gil, A. I. Colarte, A. El Ghzaoui, D. Durand, J. L. Delarbre, B. Bataille, *European Journal of Pharmaceutics and Biopharmaceutics*, **68**, 319 (2008).